ADVANCED FUNCTIONAL MATERIALS
www.afm-journal.de

Materials Views
www.MaterialsViews.com

Ultra-High Capacity Lithium-Ion Batteries with Hierarchical CoO Nanowire Clusters as Binder Free Electrodes

Kangzhe Cao, Lifang Jiao, Yongchang Liu, Huiqiao Liu, Yijing Wang, and Huatang Yuan*

Although transition metal oxide electrodes have large lithium storage capacity, they often suffer from low rate capability, poor cycling stability, and unclear additional capacity. In this paper, CoO nanowire clusters (NWCs) composed of ultra-small nanoparticles (≈10 nm) directly grown on copper current collector are fabricated and evaluated as an anode of binder-free lithium-ion batteries, which exhibits an ultra-high capacity and good rate capability. At a rate of 1 C (716 mA g^{-1}), a reversible capacity as high as 1516.2 mA h g^{-1} is obtained, and even when the current density is increased to 5 C, a capacity of 1330.5 mA h g^{-1} could still be maintained. Importantly, the origins of the additional capacity are investigated in detail, with the results suggesting that pseudocapacitive charge and the higher-oxidation-state products are jointly responsible for the large additional capacity. In addition, nanoreactors for the CoO nanowires are fabricated by coating the CoO nanowires with amorphous silica shells. This hierarchical core–shell CoO@SiO_2 NWC electrode achieves an improved cycling stability without degrading the high capacity and good rate capability compared to the uncoated CoO NWCs electrode.

1. Introduction

With the highly increasing demands for energy, many green sources of power, such as wind, tide, and solar energy, are becoming hotspots of research due to their renewability and less pollution. Nevertheless, due to their intermittence, high-efficiency energy storages need to be developed before these power sources can be fully utilized.[1] As a major device for electrical energy storage, lithium-ion batteries (LIBs) have not yet fully displayed their advantages due to their present limited capacities. For example, the classical anode material, graphite, only hosts a capacity of 372 mA h g^{-1}, far from our anticipations. In this context, it is an urgent task to explore anode materials with high capacity.[2,3]

Dr. K. Cao, Prof. L. Jiao, Dr. Y. Liu, Dr. H. Liu, Prof. Y. Wang, Prof. H. Yuan
Institute of New Energy Material Chemistry
Collaborative Innovation Center of Chemical Science and Engineering (Tianjin)
Key Laboratory of Advanced Energy Materials Chemistry (MOE)
Tianjin Key Laboratory of Metal and Molecule-based Material Chemistry
Nankai University
Tianjin 300071, P.R. China
E-mail: jiaolf@nankai.edu.cn

DOI: 10.1002/adfm.201403111

Transition metal oxides (MO_x, M: Co, Ni, Cu, Fe, etc.) possess remarkably high capacity based on the conversion mechanism ($MO_x + 2xLi + 2xe^- \leftrightarrow M + xLi_2O$) by delivering multiple electrons.[4–7] As one of the most promising anode materials for LIBs, CoO has attracted extensive interest over the last decade due to its high lithium-storage capacity (716 mA h g^{-1}).[4,8] What is disappointing is that this anode material often suffers from a large specific volume change and this often results in performance degradation. Although nanostructured materials can enlarge the capacity to some extent, a limited cycle life and inferior rate capability cannot be avoided due to the pulverization of the electrode and aggregation of the active material.[9]

Recently, two strategies have been developed to address these problems. First, carbon materials such as graphite, graphene, and carbon nanofiber/nanotube often serve as matrices to scatter CoO for improved performance.[8,10–13] The added carbon not only could act as a conductive network to enhance the electric conduction, but also acts as a buffer to accommodate the local volume changes during cycling, thus leading to improved rate capability and cycling performance. Peng et al. dispersed CoO quantum dots (3–8 nm) on graphene nanosheets and achieved a capacity of 1592 mA h g^{-1} when this composite was used as anode material in lithium ion batteries.[8] And many other excellent works also achieved high capacities larger than theoretical one. However, the origins for these high values are still unclear.[7,10–12] Another effective strategy is to fabricate nanostructured materials with hierarchical architecture. Electrodes based on hierarchical structures provide higher surface-to-volume ratios, which reduce the tendency to form agglomerates due to their larger dimensions and adequate room to accommodate the tension caused by the volume change.[2,6,14] Therefore, it is reasonable to fabricate hierarchical nanostructure CoO electrode with outstanding electrochemical performance and it is necessary to investigate the origins of the additional capacity existed to pave the way to the further study on this material.

Typically, the integrity of the electrodes is considered to be an important factor in maintaining good cycle stability.[13,15] Traditional electrode fabrication methods usually adopt polymeric binders to make the active material adhere to the current collector. The addition of inactive and insulating binders, however,

cannot ensure a nonspace connection between active material particles, also inevitably impede efforts to improve the capacity and rate capability because the insulating binders may block the pathways for lithium ion diffusion and discount the electronic conductivity. Alternatively, binder-free electrodes fabricated on current collectors could solve the shortcomings of the traditional method because of its in situ tight adhesion. The in situ synthesis techniques, such as electro-deposition, physical/chemical vapor deposition, and electrostatic spray deposition have produced many typical functional materials, however, they often need special equipments, tedious process, or corrosive gases. In contrast, the hydrothermal route may be a simple, convenient, and scale-up production one owing to its low cost, morphology controllability, and operational simplicity.[16–18]

In this paper, we have fabricated hierarchical CoO nanowire clusters (NWCs) on copper foil and directly applied it as anode of LIBs. The nanowires are composed of ultra-small nanoparticles (≈10 nm) and further self-assembled into a hierarchical structure. As expected, the hierarchical CoO NWCs electrode exhibited high lithium-storage capacity and impressive rate capability, owing to the unique hierarchical architecture with high electrode-electrolyte contact area, fast Li^+ ion diffusion, and good strain accommodation. Importantly, the origins of the additional capacity that often existed in transition metal oxide electrodes are investigated in detail, and it is confirmed that the pseudocapacitance and the higher-oxidation-state products are jointly responsible for the large additional capacity. Furthermore, a longer cycle life is achieved by uniformly coating SiO_2 on the CoO nanowires. The strategy of coating CoO NWCs with SiO_2 to enhance the cycling stability could also be extended to other materials, such as MnO_x, NiO, Fe_2O_3, CuO, etc.

2. Results and Discussion

2.1. Synthesis and Characterization

The general process for the fabrication of hierarchical CoO NWCs is illustrated in **Scheme 1** based on the scanning electron microscopy (SEM) images (Supporting Information, Figure S1) that show the products after different reaction times. Typically, Co^{2+} is chelated with F^- to transform it to $CoF_x^{(x-2)-}$ in the solution, and then the urea in the solution is decomposed into NH_3 and CO_2 by raising the temperature to about 70 °C, forming a base solution.[19] With the help of OH^- and CO_3^{2-}, Co^{2+} is slowly released from $CoF_x^{(x-2)-}$ and forms cobalt carbonate hydroxide ($Co(CO_3)_{0.5}(OH)\cdot 0.11H_2O$) nanoparticles with nucleation on the copper substrate (Supporting Information, Figure S1a). With the growth from the feedstock, many nanoflakes are formed and further self-assembled into microflowers with a three-dimensional (3D) hierarchical structure (Supporting Information, Figure S1b). As the reaction time is prolonged, the petals of the microflowers are split into nanowires by a dissolution-recrystallization process and further developed into a hierarchical structure after an "Ostwald ripening" process (Supporting Information, Figure S1c,d).[20,21] The phase structures of the precursors on the corresponding stages were also monitored by X-ray diffraction (XRD) and their patterns were shown in Supporting Information, Figure S2. It can be seen that all the diffraction peaks can be indexed to $Co(CO_3)_{0.5}(OH)\cdot 0.11H_2O$ (Joint Committee on Powder Diffraction Standards, JCPDS no. 48–083) and the diffraction intensities are becoming stronger with the reaction time prolonged. The changes of the diffraction intensities indicate that the phase of this precursor $Co(CO_3)_{0.5}(OH)\cdot 0.11H_2O$ is stable once it formed though its dimension derives from nanoparticles to microflowers and nanowire clusters. After heat-treatment in Ar atmosphere, the precursor $Co(CO_3)_{0.5}(OH)\cdot 0.11H_2O$ is converted into CoO with high crystallinity. The reactions involved may be illustrated as follows[8,19,22]

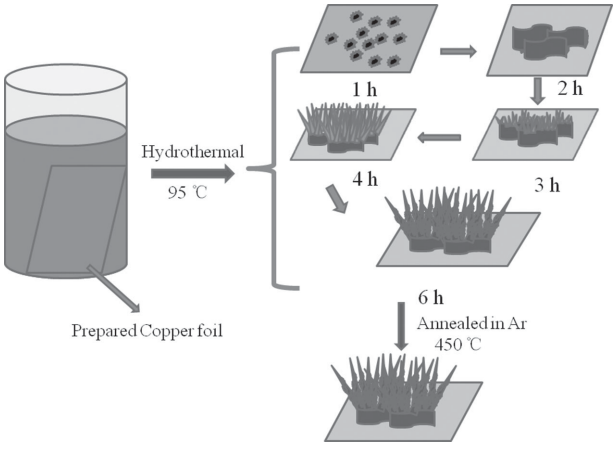

Scheme 1. Schematic illustration of the formation of hierarchical CoO NWCs on copper foil.

$$Co^{2+} + xF^- \rightarrow CoF_x^{(x-2)-} \quad (1)$$

$$CO(NH_2)_2 + H_2O \rightarrow NH_3 + CO_2 \quad (2)$$

$$CO_2 + H_2O \rightarrow CO_3^{2-} + 2H^+ \quad (3)$$

$$NH_3 \cdot H_2O \rightarrow NH_4^+ + OH^- \quad (4)$$

$$CoF_x^{(x-2)-} + 0.5CO_3^{2-} + OH^- + 0.11H_2O \rightarrow Co(CO_3)_{0.5}(OH)\cdot 0.11H_2O + xF^- \quad (5)$$

$$2Co(CO_3)_{0.5}(OH)\cdot 0.11H_2O \rightarrow 2CoO + 1.22H_2O + CO_2 \quad (6)$$

The chemical composition and valence state of the CoO NWCs have been determined by XRD and X-ray photoelectron spectroscopy (XPS). As **Figure 1**a shows, all the diffraction peaks could be well indexed to the standard for raw salt cubic CoO (JCPDS no. 48–1719), except for the two peaks originating from the copper foil (marked by *).[4,23] The XPS spectrum (Figure 1b,c) gives the binding energy of CoO. Two typical peaks, located at 795.8 and 780.1 eV in the high-resolution Co 2p spectrum, corresponded to the Co 2p1/2 and Co 2p3/2 spin-orbit peaks of CoO.[24] The O 1*s* peak at 529.5 eV (Figure 1c) is well matched with the normal Co–O bonds in the CoO lattice, while the well-resolved peak at 530.4 eV corresponds to the

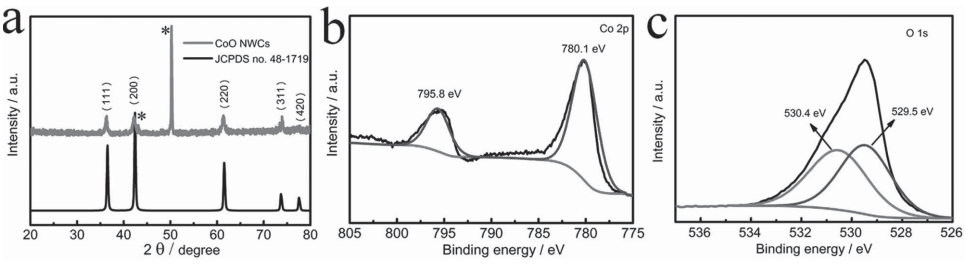

Figure 1. Typical XRD pattern a) and high-resolution XPS spectra b,c) of the hierarchical CoO NWCs on copper foil.

H–O bonds of the surface hydroxyl groups. Hydroxyl oxygen would capture electrons to produce active species, such as OH and O_2.[25] No other peaks besides those for Co, O, and C could be seen in the wide survey XPS spectrum (Supporting Information, Figure S3), providing further evidence of the purity of this material.

Figure 2a implies that the entire surface of the copper substrate is uniformly covered with CoO nanowire clusters. The cross-sectional image (Figure 2b) indicates that each nanowire has grown on the substrate to a length of 5–8 μm. Figure 2c shows a magnified SEM image of several nanowires, in which each nanowire, with a diameter of ≈150 nm, is composed of many nanoparticles ≈10 nm in size, demonstrating a hierarchical morphology. Nanoparticles with mesopores can be seen clearly in the transmission electron microscopy (TEM) image in Figure 2d, and the pore structure with large specific surface area is further probed by nitrogen isothermal adsorption–desorption measurements (Supporting Information, Figure S4), which shows type-IV isotherm and indicates the mesoporous morphology of the CoO nanowires.[7,26] Remarkably, the Brunauer–Emmett–Teller specific surface area of this material is calculated to be 58.6 m^2 g^{-1}. Unambiguously, the large specific surface area with mesopores could offer abundant active sites and facilitate electrolyte accessibility, allowing a larger lithium-ion flux and a shorter diffusion distance for lithium ions transportation when used as electrode. The well-resolved periodic lattice fringes in the high resolution TEM (HR-TEM) image with interplanar spacings of 2.13 and 1.51 Å come from the (200) and (220) planes of the raw salt cubic CoO (Figure 2e).[23] Besides, The selected area electron diffraction (SAED) patterns (Figure 2f) are exactly identical to those of the raw salt cubic CoO and can be readily matched with the (111), (200), (220), and (311) planes,[27] which are also well consistent with the XRD results.

2.2. Electrochemical Evaluation

To evaluate the lithium storage properties, the hierarchical CoO NWCs were directly used as the anode material for lithium-ion battery. The cycling performance is shown in **Figure 3**a. For the hierarchical CoO NWCs electrode, no fading tendency in capacity is observed in the first 20 cycles and a capacity of 1248.8 mA h g^{-1} still remains after 50 cycles, corresponding to 82.3% of the second cycle discharge capacity and larger than the theoretical one. The exhibition of over-theoretical capacity is a common phenomenon in nanostructured transition metal oxides tested as LIB anode materials.[4,8,10] The increasing capacity in the first 20 cycles may be due to an activation process which is caused by the enlarged surface area after a nanosize effect.[8] The decreased capacity after tens of cycles may result from the deterioration of the structure, which is an inherent characteristic for the transition metal oxide electrodes. For comparison, a conventional electrode prepared by nonself-supported hierarchical CoO NWCs, denoted as broken CoO NWCs, which was scraped off the Cu substrate shows a sharply decreasing trend in capacity, and only 440 mA h g^{-1} is retained after 50 cycles under the same conditions. The definitely superior performance of the CoO NWCs electrode may have resulted from the special structure. The voids left by the nanoparticles and the room among nanowires ensure that the active material and the electrolyte remain in intimate contact. In addition, the unique preparation method integrates the active material

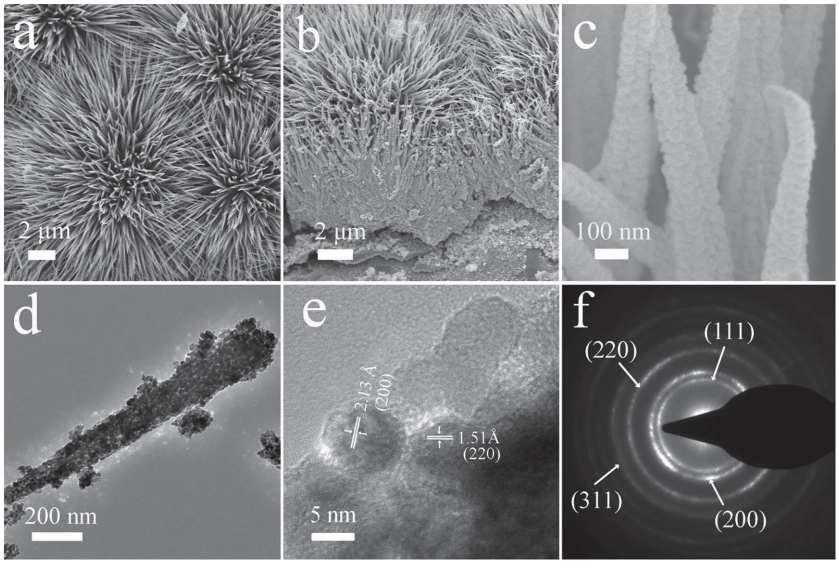

Figure 2. SEM images viewed from the top a) and in cross-section b), c) magnified SEM image of several nanowires. d) TEM image and e) HR-TEM image of a single nanowire and f) the corresponding SAED patterns.

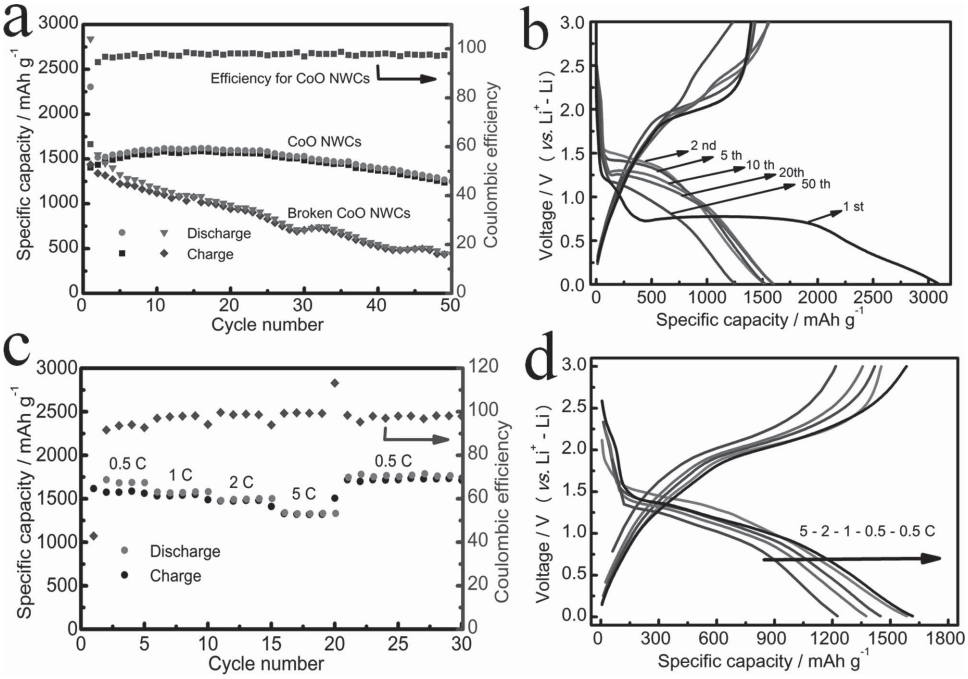

Figure 3. a) Cycling performance of binder-free electrode consisting of hierarchical CoO NWCs on copper current collector (CoO NWCs) electrode, nonself-supported CoO NWs (broken CoO NWCs) electrode at 1 C, respectively. b) The charge–discharge curves of hierarchical CoO NWCs at 1 C. c) Rate-capability performance and d) the charge–discharge curves of hierarchical CoO NWCs at different current densities.

and the current collector, which is in favor of electrons transfer. What is more, more active sites are exposed during the electrochemical activity without the need for any additive. Therefore, the virtues of the electrode prepared by this in situ method are unambiguous compared with conventional electrodes.

Figure 3b shows the galvanostatic charge–discharge curves of the CoO NWCs electrode at a current of 1 C (716 mA g^{-1}) within a voltage window of 3.0–0.01 V. It can be seen that the capacity of the first discharge reaches 3087 mA h g^{-1} and that of the first charge is 1406 mA h g^{-1}. The long stable voltage stage at 0.75 V in the first discharge is ascribed to the complex phase transformation of CoO to Co and the solid-electrolyte-interphase (SEI) formation.[12,22,28] Apart from the first cycle with a large irreversible capacity, subsequent cycles have a coulombic efficiency of almost 98%. The voltage hysteresis displayed by the following curves is a usual phenomenon for the transition metal oxide LIB anode materials and could be noted as the signature of the conversion mechanism.[29] The extra initial discharge capacity and irreversible capacity could be mainly ascribed to the formation of the SEI layer, along with other factors. The SEI layer is a gel-like film with complex components including organic layer and inorganic layer that is first formed at a low voltage (0.02–1.0 V) during the first discharge and covers the electrode.[30] In addition, the excess oxygen content in the material also could consume much Li, exhibiting an extra capacity.[31]

The rate capability is an important factor for many applications of energy storage devices, such as electric vehicles (EVs) and hybrid electric vehicles (HEVs) that require fast discharge and charge rate.[16,32] Figure 3c,d shows the rate capability performance. It can be observed that the capacity of 1685.1 mA h g^{-1} (0.5 C), 1581 mA h g^{-1} (1 C), 1479.2 mA h g^{-1} (2 C), and 1330.5 mA h g^{-1} (5 C) are obtained (with the capacity values extracted from the fifth charge–discharge cycle for each rate), respectively. More importantly, when the current density is brought back down to 0.5 C after such high current cycling, the capacity of the cell swiftly recovers and the coulombic efficiency is nearly 100%. Furthermore, the similarity of the charge and discharge curves without large voltage hysteresis changes at different current densities implies that only limited polarization exists in this system, even at large current densities, thus demonstrating an excellent rate capability. To the best of our knowledge, the excellent electrochemical performance of this material at large current densities is the best one among the reported cobalt oxide materials,[4,7,8,10,11,23] and the comparative results are listed in Supporting Information, Table S1.

Apart from the excellent rate capability, the stable capacity larger than theoretical capacity (716 mA h g^{-1} based on two electrons transfer) is another outstanding feature of this electrode. In order to understand the origins of the additional capacity, further studies were carried out. Initially, the total capacity of an electrode with the conversion mechanism can be separated into three parts: the capacity caused by the conversion reaction, the faradaic contribution from the charge transfer with surface atoms, and the nonfaradaic contribution from the double-layer effect. The latter two parts cannot be separated and are usually characterized by analyzing the relationship between the measured current (i) and the scan rate (v) from the cyclic voltammetry (CV) data.[33] The equations are listed as follows

$$i(V) = av^b \tag{7}$$

$$\lg i(V) = b \lg v + \lg a \tag{8}$$

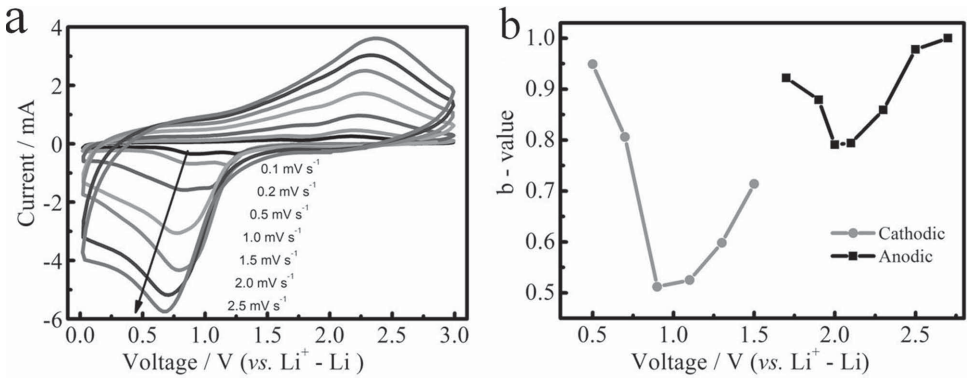

Figure 4. a) Typical CV curves at various sweep rates and b) calculated *b*-values as a function of voltage for cathodic and anodic sweeps for the hierarchical CoO NWCs electrode.

Where the measured current i obeys a power law relationship with the sweep rate v, a and b are the adjustable parameters. The b-values are determined by the slope of the plot of lg$i$ versus lg$v$, according to Equation (8). As reported by previous works,[34] the electrode is controlled by the diffusion process when the b-value is 0.5, while a capacitive response is dominant when the b-value is 1.0. The CV curves at various sweep rates and the calculated b-values for the hierarchical CoO NWCs electrode are shown in **Figure 4**. At the potentials of 0.9 and 1.1 V for the cathodic process, the b-values are 0.512 and 0.525, close to 0.5, which indicates that the charge storage mainly comes from the conversion reaction. At lower or higher potentials, however, the b-values are in the range of 0.6–1.0. This is a good indication that a part of the capacity comes from pseudocapacitive effects. During the anodic process, the b-values are in the range of 0.79–0.98, which suggests that the pseudocapacitance and conversion reaction both contribute to the capacity. Thus, pseudocapacitance plays an important role in the total capacity.

Additionally, nanosized Li_2O could act as an oxidizer for the conversion of Co^{2+} to Co^{3+} according to the work of Yu et al. and higher-oxidation-state products were formed in MnO/graphene electrode as reported by Sun et al.[35,36] Therefore, it was necessary to examine the valence state of Co ions in the fully charged products by XPS measurements in our system. As shown in **Figure 5**a, the XPS spectrum of the charged product shows that the Co 2p peaks become weaker and broader than those of the fresh CoO NWCs (Figure 1b). A pair of the characteristic peaks for Co 2p1/2 and 2p3/2 are observed at about 796.7 and 780.4 eV, corresponding to Co^{3+}.[24] Furthermore, the peaks' locations shifted to higher binding energy also indicates that the Co^{2+} is partially oxidized to a higher oxidation state (Co^{3+}).[36,37] It is believed that the improved Li reaction kinetics play a key role in the procession of Co ions are re-oxidized to a higher oxidation state by nanosized Li_2O,[36] which is confirmed by the lower charge transfer resistance at different voltages and the reduced voltage hysteresis. Figure 5b presents the electrochemical impedance spectra of the CoO NWCs electrode at different voltages in the first charge at a rate of 1 C. Each Nyquist plot consists of a depressed semicircle (at high frequency) due to charge-transfer resistance and a linear part (at low frequency) due to Warburg resistance. The smaller and smaller charge-transfer resistance at different charge stages indicates that the Li reaction kinetics is improving with the rising voltage. In addition, the lower voltage hysteresis after the first cycle (Figure 5c) is also evidence for the improved kinetics.[38] Thus, it is reasonable that the Co^{2+} in fresh CoO NWCs electrode could be oxidized to Co^{3+} after the electrode is fully charged owing to the improved reaction kinetics.

Based on the pseudocapacitance contributions and higher-oxidation-state products, a stable high capacity and good rate capability are obtained in this binder free hierarchical CoO NWCs electrode. However, the cycle stability is not satisfied. And the morphology collapse may account for this

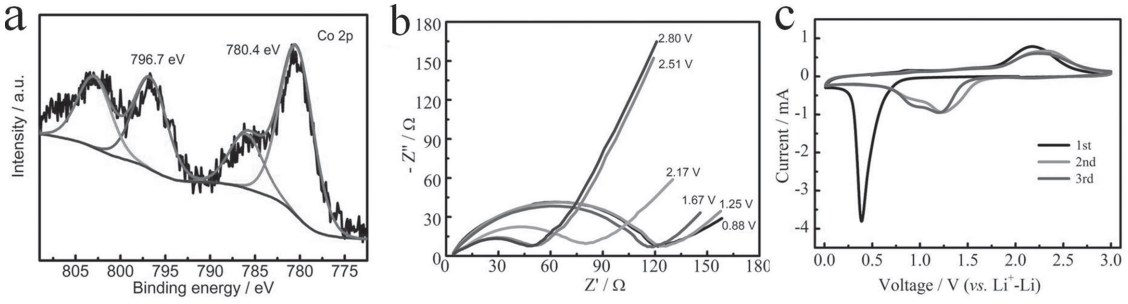

Figure 5. a) High-resolution Co 2p XPS spectrum of the hierarchical CoO NWCs electrode in the fully charged state at 1 C. b) Electrochemical impedance spectra of the CoO NWCs electrode in the first charge at 1 C over the frequency range from 100 kHz to 0.1 Hz. c) CV curves of the CoO NWCs with a scan rate of 0.1 mV s^{-1}.

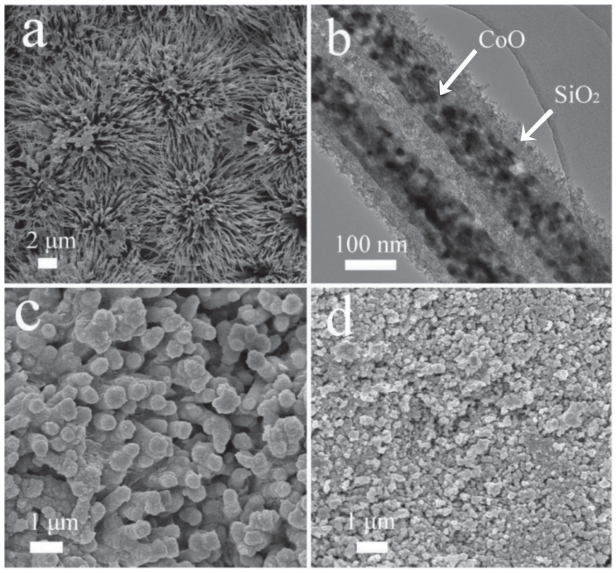

Figure 6. SEM a) and TEM b) images of hierarchical CoO@SiO_2 NWCs; SEM images of hierarchical CoO@SiO_2 NWCs electrode c) and CoO NWCs electrode d) after 50 cycles at 1 C.

phenomenon. Recently, Wu et al. designed a novel double-walled Si–SiO_x nanotube anode, in which the inner wall was active silicon and the outer wall was confining SiO_x.[39] As one important factor in the excellent cycling stability (more than 6000 cycles with 88% capacity retention), the SiO_x shell of the silicon nanotube is attributed to the development of a stable SEI layer and enabling the inner silicon to expand inward into the hollow space owing to its mechanically rigidity. Additionally, the SiO_x shell allows lithium ions to pass through. However, the precursor SiH_4 used in their work is not safe and the chemical vapour deposition method needs specific equipment and is not effective enough. Thus, it is reasonable to confine the active materials with large volume expansion in the SiO_x shell to achieve a long cycle life by a facile and simple method. In our work, an environmental friendly and safe precursor tetraethyl orthosilicate (TEOS) has been employed as silica source and low temperature hydrothermal reaction was adopted for the synthesis. As displayed by **Figure 6**a,b, the CoO nanowires are uniformly coated with amorphous SiO_2, and the XRD patterns, Fourier transform infrared spectra (FT-IR), and HR-TEM image in Supporting Information, Figure S5 further confirm that CoO NWCs do not change after the coating with SiO_2. Figure 6c,d shows the morphology of the CoO@SiO_2 NWCs and CoO NWCs electrodes after 50 cycles. Compared with the CoO NWCs electrode, in which the nanowires have collapsed and are transformed into nanoparticles after 50 cycles (Figure 6d), the core-shell structure of the CoO@SiO_2 NWCs electrode (Figure 6c) keeps its morphology, and the SiO_2 shell successfully prevents the nanowires from collapsing. As depicted by **Figure 7**, the CoO@SiO_2 NWCs electrode exhibits a longer cycle life without degrading the high capacity and good rate capability compared to the CoO NWCs electrode. Meanwhile, the thickness of the silica shell could be controlled by adjusting the concentration of TEOS and that has an important effect on the LIB performance. As shown in Supporting Information, Figure S6, a thin SiO_2 shell could extend the cycling performance in some way, while the sample with thicker silica shell exhibits a lower capacity though its cycle stability is perfect. Therefore, the strategy of coating CoO nanowire with SiO_2 is effective for gaining a longer cycle life and its simplicity and convenience to be duplicated make it widely adopt on other metal oxide anode materials.

Based on the results discussed above, our unique hierarchical CoO NWCs manifest greatly enhanced lithium storage properties with high reversible capacity and remarkable high-rate performance. These outstanding properties are believed to be benefits of the unique hierarchical architecture.[18,22,40] First of all, the integration of the CoO NWCs and the current collector provides tight adhesion, ensuring that the active material does not peel off from the current collector, which theoretically facilitates electrons transfer between the substrate and the NWCs. Second, the open and hierarchical architecture without binder clapped could afford sufficient active sites to participate in electrochemical activity during the charge–discharge process. What is more, the nanowire array configuration can allow the electrolyte to penetrate conveniently, keeping each CoO nanowire not only in contact with the copper current collector but also surrounded by the electrolyte solution. When added the lots of voids left by the nanoparticles which construct the nanowire, a net way for the electrolyte to diffuse fast is formed. This feature is vital to high rate capability. In addition, by coating the nanowire with SiO_2, a nanoshell for the electrochemical reaction is established. In this way, the inner CoO nanowires can only expand into the voids between the nanoparticles, avoiding collapse. Thus, the morphology of the hierarchical nanowires is retained, giving this electrode superior cycle life.

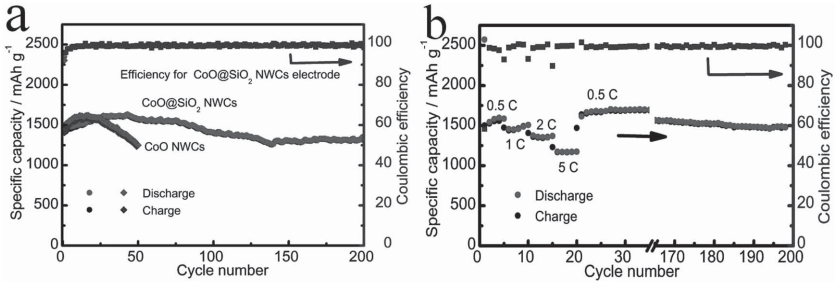

Figure 7. a) Cycling performances of hierarchical CoO NWCs and CoO@SiO_2 NWCs electrodes at 1 C and b) the rate performance of CoO@SiO_2 NWCs electrode.

3. Conclusions

In summary, hierarchical CoO NWCs directly grown on copper foil were synthesized and showed high capacity and excellent rate capability when investigated as LIB anode material. The origins of the additional capacity, as demonstrated in the discussion, provide a clean explanation for the over-theoretical capacity that exists in conversion-electrode material. Furthermore, the strategy of coating

CoO NWCs with SiO_2 to enhance the cycling stability could be extended to other materials, such as MnO_x, NiO, Fe_2O_3, CuO, etc. We believe that the obtained encouraging electrochemical results and scientific understanding could pave the way to further study of conversion-electrodes.

4. Experimental Section

Preparation of Hierarchical CoO NWCs and CoO@SiO_2 NWCs: All chemical reagents were purchased from J&K without any further purification. The hierarchical CoO nanowire clusters were synthesized by a modified two-step method involving hydrothermal and annealing treatments.[19,23] The copper current collector (0.8×5 cm^2) was cleaned with ethanol, HNO_3 solution, ethanol, sequentially for 10 min in an ultrasonic bath, respectively, and then dried at room temperature, before being accurately weighted. The reaction solution was obtained by dissolving $Co(NO_3)_2{\cdot}6H_2O$ (5 mmol), LiF (5 mmol), and urea (25 mmol) in deionized water (70 mL), and the resultant solution was then transferred into a Teflon-lined stainless steel autoclave (100 mL). The as-prepared copper foil was then put into the solution and leaned against the autoclave. After the autoclave was maintained at 95 °C for 6 h, the copper foil with the precursor was fetched out and rinsed by distilled water and ethanol several times. To obtain the ultimate product, the precursor was annealed at 450 °C in Ar atmosphere for 4 h. The mass loading of the hierarchical CoO NWCs was about 0.95 mg cm^{-2} on copper substrate, as calculated by the difference method on a microbalance (Mettler, XS105DU) with an accuracy of 0.01 mg. In order to investigate the formation process, the intermediate products were collected after different reaction times of 1, 2, 3, and 4 h. For comparison, nonself-supported hierarchical CoO NWCs were prepared by scraping them from the copper foil. As in the conventional process, the comparison sample was mixed with Super-P Li and polyvinylidene fluoride (PVDF) (8:1:1 in weight) smeared on the same copper foil as the anode electrode (this sample is simply denoted as broken CoO NWCs electrode). In order to coat the nanowires with SiO_2 shells, the CoO nanowires were immersed in a mixed solution containing cetyltrimethylammonium bromide (CTAB, 0.050 g), deionized water (40 mL), concentrated ammonia aqueous solution (0.5 mL, 28 wt%), tetraethyl orthosilicate (TEOS, 0.5 mL), and ethanol (30 mL).[41] After being maintained at 80 °C for 4 h in a teflon-lined stainless steel autoclave, the products were thoroughly rinsed with distilled water and dried. For the control tests, the amount of TEOS was set as 0.1 mL and 1.0 mL with other conditions unchanged.

Materials Characterization: The crystal structures of the products were characterized by X-ray di raction (XRD, Rigaku MiniFlex II, with Cu Kα radiation, $\lambda = 1.5408$ Å). The morphology and microstructure were characterized by scanning electron microscopy (SEM, JEOL JSM7500) and transmission electron microscopy (TEM, JEOL-2100F, 200 kV), as well as X-ray photoelectron spectroscopy (XPS, PHI 5000 Versaprobe, ULVAC PHI) invested the valence of ions. Surface area was measured by the N2 adsorption-desorption isotherms on a BELSORP-mini instrument at 77 K.

Electrochemical Measurements: Electrochemical performance testing was carried out using a two-electrode cell assembled in an argon-filled glove box with the moisture and oxygen content maintained below 1.0 ppm. The hierarchical CoO NWCs and CoO@SiO_2 NWCs on copper foil were directly used as the working electrode, and pure Li foil was the counter electrode, while the separator was Celgard 2320 membrane. 1 M $LiPF_6$ in a mixture of ethylene carbonate (EC) and dimethyl carbonate (DMC) (EC: DMC = 1:1 by volume) was used as the electrolyte. The cells were aged for 6 h before measurement. Cyclic voltammogram (CV) tests with a cut-off voltage window of 0.01–3.0 V (vs Li^+-Li, with a scanning rate of 0.1 mV s^{-1}) and electrochemical impedance spectroscopy (EIS) measurements both were performed on a CHI660 b electrochemical workstation (Chenhua, Shanghai, China). The galvanostatic charge–discharge tests were carried out using a Land Battery Measurement system (Land CT2001A, China) at various current densities of 0.5–5 C in the fixed voltage window of 3.0–0.01 V at room temperature. The comparison cell was assembled and tested under the same conditions.

Supporting Information

Supporting Information is available from the Wiley Online Library or from the author.

Acknowledgements

This work was financially supported by the 973 Program (2010CB631303), the National Natural Science Foundation of China (NSFC) (51231003), the Ministry of Education (MOE) of China (IRT-13R30 and IRT-13022), and the 111 Project (B12015).

Received: September 9, 2014
Revised: November 19, 2014
Published online: January 12, 2015

[1] W. Tang, Y. S. Zhu, Y. Y. Hou, L. L. Liu, Y. P. Wu, K. P. Loh, H. P. Zhang, K. Zhu, *Energy Environ. Sci.* **2013**, *6*, 2093.
[2] J. Jiang, Y. Y. Li, J. P. Liu, X. T. Huang, C. Z. Yuan, X. W. Lou, *Adv. Mater.* **2012**, *24*, 5166.
[3] a) W. W. Lee, J. M. Lee, *J. Mater. Chem. A* **2014**, *2*, 1589; b) B. L. Ellis, P. Knauth, T. Djenizian, *Adv. Mater.* **2014**, *26*, 3368.
[4] a) H. Guan, X. Wang, H. Q. Li, C. Y. Zhi, T. Y. Zhai, Y. Bando, D. Golberg, *Chem. Commun.* **2012**, *48*, 4878; b) J. S. Chen, T. Zhu, Q. H. Hu, J. J. Gao, F. B. Su, S. Z. Qiao, X. W. Lou*ACS Appl. Mater. Interfaces* **2010**, *2*, 3628.
[5] P. Poizot, S. Laruelle, S. Grugeon, L. Dupont, J. M. Tarascon, *Nature* **2000**, *407*, 496.
[6] J. S. Luo, X. H. Xia, Y. S. Luo, C. Guan, J. L. Liu, X. Y. Qi, C. F. Ng, T. Yu, H. Zhang, H. J. Fan, *Adv. Energy Mater.* **2013**, *3*, 737.
[7] a) Y. M. Sun, X. L. Hu, W. Luo, Y. H. Huang, *J. Mater. Chem.* **2012**, *2*, 13826; b) X. W. Lou, D. Deng, J. Y. Lee, L. A. Arche, *J. Mater. Chem.* **2008**, *18*, 4397.
[8] a) C. X. Peng, Y. Qin, S. H. Yang, C. Z. Li, Y. H. Zuo, S. Y. Liu, J. H. Yang, *ACS Nano* **2012**, *6*, 1074; b) S. L. Xiong, J. S. Chen, X. W. Lou, H. C. Zeng, *Adv. Funct. Mater.* **2012**, *22*, 861.
[9] a) L. Yu, L. Zhang, H. B. Wu, G. Q. Zhang, X. W. Lou, *Energy Environ. Sci.* **2013**, *6*, 2664; b) S. H. Lee, S. H. Yu, J. E. Lee, A. H. Jin, D. J. Lee, N. Lee, H. Jo, K. Shin, T. Y. Ahn, Y. W. Kim, H. Choe, Y. E. Sung, T. Hyeon, *Nano Lett.* **2013**, *13*, 4249.
[10] W. H. Ryu, J. Shin, J. W. Junga, I.-D. Kim, *J. Mater. Chem. A* **2013**, *1*, 3239.
[11] Y. M. Sun, X. L. Hu, W. Luo, Y. H. Huang, *J. Phys. Chem. C* **2012**, *116*, 20794.
[12] F. D. Wu, Y. Wang, *J. Mater. Chem.* **2011**, *21*, 6636.
[13] X. L. Huang, R. Z. Wang, D. Xu, Z. L. Wang, H. G. Wang, J. J. Xu, Z. Wu, Q. C. Liu, Y. Zhang, X. B. Zhang, *Adv. Funct. Mater.* **2013**, *23*, 4345.
[14] a) A. Q. Pan, H. B. Wu, L. Zhang, X. W. Lou, *Energy Environ. Sci.* **2013**, *6*, 1476; b) D. P. Volanti, A. A. Felix, M. O. Orlandi, G. Whitfield, D. J. Yang, E. Longo, H. L Tuller, J. A. Varela, *Adv. Funct. Mater.* **2013**, *23*, 1759; c) H. G. Wang, D. L. Ma, X. L. Huang, Y. Huang, X. B. Zhang, *Sci. Rep.* **2012**, *2*, 701; d) K. Gerasopoulos, E. Pomerantseva, M. McCarthy, A. Brown, C. S. Wang, J. Culver, R. Ghodssi, *ACS Nano* **2012**, *6*, 6422.
[15] S. Hariharan, K. Saravanan, V. Ramar, P. Balaya, *Phys. Chem. Chem. Phys.* **2013**, *15*, 2945.

[16] S. C. Zhang, Z. J. Du, R. X. Lin, T. Jiang, G. R. Liu, X. M. Wu, D. S. Weng, *Adv. Mater.* **2010**, *22*, 5378.
[17] a) M. Zhong, Y. Sato, M. Kurniawan, A. Apostoluk, B. Masenelli, E. Maeda, Y. C. Ikuhara, J. J. Delaunay, *Nanotechnology* **2012**, *23*, 495602; b) Y. H. Liu, Y. H. Xu, Y. J. Zhu, J. N. Culver, C. A. Lundgren, K. Xu, C. S. Wang, *ACS Nano* **2013**, *7*, 3627.
[18] Y. G. Li, B. Tan, Y. Y. Wu, *Nano Lett.* **2008**, *8*, 265.
[19] J. Jiang, J. P. Liu, X. T. Huang, Y. Y. Li, R. M. Ding, X. X. Ji, Y. Y. Hu, Q. B. Chi, Z. H. Zhu, *Crystal Growth Des.* **2010**, *10*, 70.
[20] Y. Sun, C. S. Li, L. N. Wang, Y. Z. Wang, X. G. Ma, P. J. Ma, M. Y. Song, *RSC Adv.* **2012**, *2*, 8110.
[21] a) N. T. K. Thanh, N. Maclean, S. Mahiddine, *Chem. Rev.* **2014**, *114*, 7610; b) J. B. Lian, X. C. Duan, J. M. Ma, P. Peng, T. Kim, W. J. Zheng, *ACS Nano* **2009**, *3*, 3749.
[22] X. H. Xia, J. P. Tu, Y. Q. Zhang, J. Chen, X. L. Wang, C. D. Gu, C. Guan, J. S. Luo, H. J. Fan, *Chem. Mater.* **2012**, *24*, 3793.
[23] J. Jiang, J. P. Liu, R. M. Ding, X. X. Ji, Y. Y. Hu, X. Li, A. Z. Hu, F. Wu, Z. H. Zhu, X. T. Huang, *J. Phys. Chem. C* **2010**, *114*, 929.
[24] T. L. Barr, *J. Phys. Chem.* **1978**, *82*, 1801.
[25] a) X. G. Hou, K. Yao, X. M. Wang, D. J. Li, B. Liao, *Vacuum* **2014**, *100*, 74; b) V. M. Jimenez, A. Fernandez, J. P. Espinos, A. R. Gonzalez-Elipe, *J. Electron Spectrosc. Relat. Phenom.* **1995**, *71*, 61; c) C. Z. Yuan, J. Y. Li, L. R. Hou, L. Yang, L. F. Shen, X. G. Zhang, *J. Mater. Chem.* **2012**, *22*, 16084.
[26] S. M. Guo, G. X. Lu, S. Qiu, J. R. Liu, X. Z. Wang, C. Z. He, H. G. Wei, X. R. Yan, Z. H. Guo, *Nano Energy* **2014**, *9*, 41.
[27] K. M. Nam, J. H. Shim, D. W. Han, H. S. Kwon, Y. M. Kang, Y. Li, H. Song, W. S. Seo, J. T. Park, *Chem. Mater.* **2010**, *22*, 4446.
[28] R. H. Wang, C. H. Xu, J. Sun, Y. Q. Liu, L. Gao, C. S. Lin, *Nanoscale* **2013**, *5*, 6960.
[29] Y. Wang, H. Xia, L. Lu, J. Y. Lin, *ACS Nano* **2010**, *4*, 1425.
[30] a) S. Chattopadhyay, A. L. Lipson, H. J. Karmel, J. D. Emery, T. T. Fister, P. A. Fenter, M. C. Hersam, M. J. Bedzyk, *Chem. Mater.* **2012**, *24*, 3038; b) S. Laruelle, S. Grugeon, P. Poizot, M. Dollé, L. Dupont, J. M. Tarascon, *J. Electrochem. Soc.* **2002**, *149*, A627.
[31] C. H. Chen, B. J. Hwang, J. S. Do, J. H. Weng, M. Venkateswarlu, M. Y. Cheng, R. Santhanam, K. Ragavendran, J. F. Lee, J. M. Chen, D. G. Liu, *Electrochem. Commun.* **2010**, *12*, 496.
[32] L. Huang, D. C. Chen, Y. Ding, S. Feng, Z. L. Wang, M. L. Liu, *Nano Lett.* **2013**, *13*, 3135.
[33] T. Brezesinski, J. Wang, J. Polleux, B. Dunn, S. H. Tolber, *J. Am. Chem. Soc.* **2009**, *131*, 1802.
[34] a) P. F. Yu, C. L. Li, X. X. Guo, *J. Phys. Chem. C* **2014**, *118*, 10616; b) K. Zhu, Q. Wang, J. H. Kim, A. A. Pesaran, A. J. Frank, *J. Phys. Chem. C* **2012**, *116*, 11895.
[35] Y. Yu, C. H. Chen, J. L. Shui, S. Xie, *Angew. Chem. Int. Ed.* **2005**, *44*, 7085.
[36] Y. M. Sun, X. L. Hu, W. Luo, F. F. Xia, Y. H. Huang, *Adv. Funct. Mater.* **2013**, *23*, 2436.
[37] Y. Xia, Z. Xiao, X. Dou, H. Huang, X. H. Lu, R. J. Yan, Y. P. Gan, W. J. Zhu, J. P. Tu, W. K. Zhang, X. Y. Tao, *ACS Nano* **2013**, *7*, 7083.
[38] a) H. Jiang, Y. J. Hu, S. J. Guo, C. Y. Yan, P. S. Lee, C. Z. Li, *ACS Nano* **2014**, *8*, 6038; b) Y. J. Mai, D. Zhang, Y. Q. Qiao, C. D. Gu, X. L. Wang, J. P. Tu, *J. Power Sources* **2012**, *216*, 201.
[39] H. Wu, G. Chan, J. W. Choi, I. Ryu, Y. Yao, M. T. McDowell, S. W. Lee, A. Jackson, Y. Yang, L. B. Hu, Y. Cui, *Nat. Nanotech.* **2012**, *7*, 310.
[40] a) L. Hu, H. Zhong, X. R. Zheng, Y. M. Huang, P. Zhang, Q. W. Chen, *Sci. Rep.* **2012**, *2*, 986; b) J. C. Liu, Y. J. Xu, X. J. Ma, J. K. Feng, Y. T. Qian, S. L. Xiong*Nano Energy* **2014**, *7*, 52.
[41] Y. H. Deng, D. W. Qi, C. H. Deng, X. M. Zhang, D. Y. Zhao, *J. Am. Chem. Soc.* **2008**, *130*, 28.